Inorganic Chemistry

ARTICLE

pubs.acs.org/IC

Metal Ion-Controlled Self-Assembly Using Pyrimidine Hydrazone Molecular Strands with Terminal Hydroxymethyl Groups: A Comparison of Pb(II) and Zn(II) Complexes

Daniel J. Hutchinson, Lyall R. Hanton,* and Stephen C. Moratti

Department of Chemistry, University of Otago, P.O. Box 56, Dunedin, New Zealand

Supporting Information

ABSTRACT: Metal complexation studies were performed with the ditopic pyrimidine−hydrazone (pym−hyz) strand 6-hydroxymethylpyridine-2-carboxaldehyde (2-methyl-pyrimidine-4,6-diyl)bis(1-methylhydrazone) (**1**) and $Pb(ClO_4)_2\cdot 3H_2O$, $Pb(SO_3CF_3)_2\cdot H_2O$, $Zn(SO_3CF_3)_2$, and $Zn(BF_4)_2$ to examine the ability of **1** to form various supramolecular architectures. X-ray crystallographic and NMR studies showed that coordination of the Pb(II) salts with **1** on a 2:1 metal/ligand ratio in CH_3CN and CH_3NO_2 resulted in the linear complexes $[Pb_2\mathbf{1}(ClO_4)_4]$ (**2**), $[Pb_2\mathbf{1}(ClO_4)_3(H_2O)]ClO_4$ (**3**), and $[Pb_2\mathbf{1}(SO_3CF_3)_3(H_2O)]SO_3CF_3$ (**4**). Two unusually distorted [2 × 2] grid complexes, $[Pb\mathbf{1}(ClO_4)]_4(ClO_4)_4$ (**5**) and $[Pb\mathbf{1}(ClO_4)]_4(ClO_4)_4\cdot 4CH_3NO_2$ (**6**), were formed by reacting $Pb(ClO_4)_2\cdot 6H_2O$ and **1** on a 1:1 metal/ligand ratio in CH_3CN and CH_3NO_2. These grids formed despite coordination of the hydroxymethyl arms due to the large, flexible coordination sphere of the Pb(II) ions. A [2 × 2] grid complex was formed in solution by reacting $Pb(SO_3CF_3)_2\cdot H_2O$ and **1** on a 1:1 metal/ligand ratio in CH_3CN as shown by ^1H NMR, microanalysis, and ESMS. Reacting the Zn(II) salts with **1** on a 2:1 metal/ligand ratio gave the linear complexes $[Zn_2\mathbf{1}(H_2O)_4](SO_3CF_3)_4\cdot C_2H_5O$ (**7**) and $[Zn_2\mathbf{1}(BF_4)(H_2O)_2(CH_3CN)](BF_4)_3\cdot H_2O$ (**8**). ^1H NMR studies showed the Zn(II) and Pb(II) ions in these linear complexes were labile undergoing metal ion exchange. All of the complexes exhibited pym−hyz linkages in their cisoid conformation and binding between the hydroxymethyl arms and the metal ions. No complexes were isolated from reacting either of the Zn(II) salts with **1** on a 1:1 metal/ligand ratio, due to the smaller size of the Zn(II) coordination sphere as compared to the much larger Pb(II) ions.

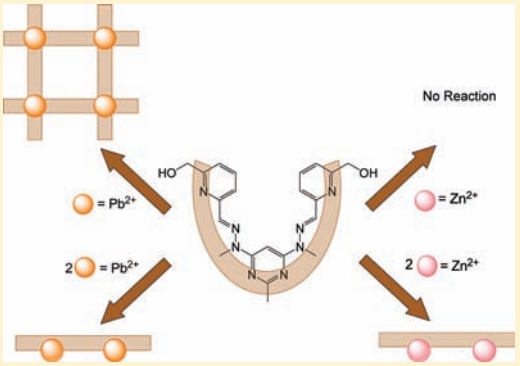

INTRODUCTION

The C═N bond of the hydrazone motif is capable of undergoing a dynamic structural change due to the incidence of a range of external stimuli including photochemical and thermal triggers[1] as well as metal ion coordination.[2] As a result, molecular strands comprised of alternating hydrazone (hyz) and heterocyclic (het) units such as pyrimidine (pym),[3] pyrazine (py),[4] and triazine[5] have been extensively studied. These strands exhibit several attractive attributes including (1) their convenient synthesis by the condensation of hydrazine and aldehyde derivatives of the desired heterocycles,[3] (2) their ability to undergo significant, and reversible, changes in shape upon coordination of suitable metal ions,[2] and (3) the high level of customization available through the choice of heterocycle, which influences both the original shape of the strand and the motion of isomerization.[4] They show potential applications in the realm of nanotechnology devices[6] such as metal controlled sensors and actuators,[7] molecular tweezers,[8] and devices intended for information storage.[9]

Of particular interest is the pyrimidine−hydrazone (pym−hyz) motif, which acts as a helicity codon, as a result of the C═N hydrazone bond's strong preference for a transoid conformation and the stabilizing effects of $\pi-\pi$ stacking interactions between the heterocyclic rings of a helical pym−hyz strand.[3,10] Coordination with suitable metal ions, however, causes the hydrazone linkage to rotate to the cisoid conformation to present a tridentate coordination site for the incoming metal ion, which results in the uncoiling of the pym−hyz strand to form a linear complex. This uncoiling motion corresponds to a one-dimensional nanomechanical motion.[2,5]

Our research interests concern the use of the reversible expansion and contraction motion of the pym−hyz strands to drive macroscopic devices. The first step toward this goal was to synthesize the ditopic ligand **1**, which contains 6-hydroxymethyl groups on the terminal pyridine (py) rings.[11] Chemical manipulation of these functional groups is one route to incorporating pym−hyz strands into larger chemical systems, such as polymer gel actuators and sensors.[7,12] A large variety of substituents have been added to pym−hyz strands in the past, particularly on the C2 position of the pyrimidine rings, the ternary N-site of the

Received: March 31, 2011
Published: July 13, 2011

hydrazine groups, and on the C atoms of the pyridine rings, which typically terminate the molecular strands.[2,3,13−15] However, the position of the hydroxymethyl arms in **1** on C6 of the pyridine rings, which is the optimum position for polymer gel formation, results in the placement of the O donor atom such that it may form a chelate ring with a metal ion bound to the pyridine and hydrazone N donors and therefore complicates the coordination chemistry of these systems.[16,17] It is therefore necessary to evaluate the impact the appended hydroxymethyl groups have on the interaction between the pym−hyz units in **1** and various metal ions, both in terms of the supramolecular architectures that can be produced and whether the hydroxymethyl arms inhibit the transoid to cisoid conformational change.

Previous reactions between **1** and Cu(II) ions showed frequent binding of the hydroxymethyl arms to the Cu(II) ions as well as extensive intermolecular H-bonding between adjacent complexes and counterions through the terminal OH groups.[11] These interactions did not inhibit the transoid to cisoid conformational change upon the coordination of Cu(II), as **1** did change shape from horseshoe to linear upon reacting with a two molar equivalence of Cu(II) ions. It was significant, however, that the binding of the hydroxymethyl arms to Cu(II) did prevent the formation of [2 × 2] square grids, which are usually the result when pym−hyz strands are reacted with ions such as Cu(II),[13] Hg(II),[18] Pb(II),[2] and Zn(II),[15,19] on a 1:1 metal/ligand ratio. With **1** the 1:1 reactions resulted in bent monocopper complexes, which contained one occupied coordination site and one empty site that consequently had retained its original transoid shape. Grid formation was inhibited due to the binding of the hydroxymethyl arm to the Cu(II) ion in the occupied site saturating the coordination sphere of the Cu(II) ion, thus preventing the accommodation of further molecules of **1**. Therefore, the appended hydroxymethyl arms offer a degree of control over the self-assembly of ligand **1** and Cu(II) ions.[11]

To explore further the influence of the hydroxymethyl arms on the coordination chemistry of pym−hyz strands, **1** was reacted with salts of Pb(II) and Zn(II) in 2:1 and 1:1 metal/ligand ratios. We hypothesize that it is possible for Pb(II) to form a [2 × 2] grid as it is known to have a large and flexible coordination sphere,[20] which may be able to accommodate two molecules of **1** despite possible interference from the hydroxymethyl arms. While Zn(II) has been used to successfully create [2 × 2] square grids with other pym−hyz strands,[2,15,19] like Cu(II) we expected grid formation to be inhibited by the presence of the hydroxymethyl arms, due to the small coordination sphere of Zn(II). Importantly, both metals are diamagnetic, allowing the coordination reactions with **1** to be characterized in solution phase, in addition to X-ray crystallography providing solid-state structures.

Herein, we report the Pb(II) and Zn(II) complexes of **1** obtained in both the solid state and the solution phase to test our hypothesis that grid formation is possible with Pb(II) but not with Zn(II) ions. The addition of $Pb(ClO_4)_2 \cdot 3H_2O$ and $Pb(SO_3CF_3)_2 \cdot H_2O$ to **1** in a 2:1 metal/ligand ratio in CH_3CN and CH_3NO_2 resulted in linear complexes, with each of the pym−hyz bonds in their cisoid conformation. All of these linear Pb(II) complexes showed binding of both hydroxymethyl arms to the Pb(II) ion present in the pym−hyz−py coordination pocket both in solution and in the solid state. $Pb(ClO_4)_2$ was also reacted with **1** in a 1:1 metal/ligand ratio in both CH_3CN and CH_3NO_2, resulting in the formation of isomorphous [2 × 2] square grid complexes. These grids were unusually distorted as a result of the ligand backbone being twisted due to the hydroxymethyl arms crowding the coordination sphere of the Pb(II) ions. NMR studies showed the grid was present as the only species in solution.

Reacting **1** with $Zn(SO_3CF_3)_2$ and $Zn(BF_4)_2$ in a 2:1 metal/ligand ratio also resulted in linear complexes with cisoid hydrazone linkages. Both of the hydroxymethyl arms of the 2:1 $Zn(SO_3CF_3)_2$ complex were coordinated to Zn(II) ions, while the 2:1 $Zn(BF_4)_2$ complex had one arm coordinated at all times and the other arm was disordered such that it was only bound part of the time. Reacting **1** with the Zn(II) salts in a 1:1 ratio in CH_3CN resulted in dissolution of **1**, although NMR studies of the reaction in CD_3CN showed nothing other than uncoordinated **1** in solution. Over time, **1** would precipitate out of solution, suggesting that the Zn(II) ions were labile and were unable to form a 1:1 complex. ^{1}H NMR experiments involving the titration of the Zn(II) and Pb(II) 2:1 metal/ligand complexes with either Pb(II) or Zn(II) metal ions showed that the ions in these complexes were labile and could freely exchange between molecules of **1**, producing an equilibrium mixture that contained the linear heterometallic complex.

EXPERIMENTAL SECTION

General. All chemicals were used as received without further purification. Ligand **1** was prepared according to the literature method.[11] $Pb(ClO_4)_2 \cdot 3H_2O$, $Zn(SO_3CF_3)_2$, and $Zn(BF_4)_2 \cdot H_2O$ were acquired from Aldrich. $Pb(SO_3CF_3)_2 \cdot H_2O$ was synthesized through treatment of $PbCO_3 \cdot Pb(OH)_2$ with HSO_3CF_3. All solvents were of LR grade or above.

Microanalyses were carried out in the Campbell Microanalytical Laboratory, University of Otago. All measured microanalysis results had an uncertainty of ±0.4%. ^{1}H and ^{13}C NMR spectra and two-dimensional (gCOSY, NOSEY, HSQC, gHMBC) spectra were collected on a 500 MHz Varian UNITY INOVA spectrometer at 298 K. Spectra were collected in CD_3CN and were referenced to the internal solvent signal, with chemical shifts reported in δ units (ppm). Electrospray mass spectrometry (ESMS) was carried out on a Bruker micro-TOFQ instrument (Bruker Daltronics, Bremen, Germany). Samples were introduced using direct infusion into an ESI source in positive mode. Sampling was averaged for 2 min over a m/z range of 50−3000 amu. The mass was calibrated using an external calibrant of sodium formate clusters, 15 calibrations points from 90 to 1050 amu, using a quadratic plus HPC line fit. ESMS spectra were processed using Compass software (version 1.3 Bruker Daltronics, Bremen, Germany). Infrared (IR) spectra were recorded on a Perkin-Elmer Spectrum BX FT-IR system. Samples were prepared as KBr discs.

Caution! *Although no problems were encountered in this work, transition metal perchlorates are potentially explosive. They should be prepared in small amounts and handled with care.*

$Pb_2$1$(ClO_4)_4$. $Pb(ClO_4)_2 \cdot 3H_2O$ (45.2 mg, 0.098 mmol) in CH_3CN (2 mL) was added to **1** (20.4 mg, 0.049 mmol), resulting in partial dissolution of **1** and the formation of a yellow solution. This mixture was stirred at room temperature until all the solid had dissolved. Diethyl ether was slowly diffused into this solution, resulting in the formation of yellow crystals. These crystals were filtered and dried in vacuo to yield Pb_2**1**$(ClO_4)_4$ as a yellow solid (25.9 mg, 43%). Anal. Calcd for $C_{21}H_{24}N_8O_{18}Cl_4Pb_2$: C, 20.45; H, 1.96; N, 9.09. Found: C, 20.30; H, 1.94; N, 8.82. ^{1}H NMR (CD_3CN, 500 MHz) δ/ppm: 8.74 (2H, s, H9), 8.28 (2H, t, J = 7.8 Hz, H12), 7.96 (2H, d, J = 7.5 Hz, H11), 7.71 (2H, d, J = 7.9 Hz, H13), 6.61 (1H, s, H5), 5.75 (2H, s, H17), 5.34 (4H, s, H15), 3.73 (6H, s, H8), 2.86 (3H, s, H9). ^{13}C NMR (500 MHz, CD_3CN) δ/ppm: 168.38 (C2), 162.73 (C14), 161.64 (C4,6), 150.73 (C10), 144.56 (C9), 142.45 (C12), 128.62 (C13), 125.63 (C11), 87.69 (C5), 65.76

dx.doi.org/10.1021/ic200670w |*Inorg. Chem.* 2011, 50, 7637–7649

(C15), 36.34 (C8), 26.86 (C7). ESMS m/z found: 627.17356. Calcd for $C_{21}H_{23}N_8O_2Pb^+$: 627.17072. Selected IR (KBr disk) ν/cm^{-1}: 3406 (s, br, OH str), 1589 (s), 1550 (s, C═N str), 1486 (m), 1438 (m), 1385 (m), 1295 (s), 1163−1047 (s, br). Crystals suitable for X-ray determination were grown by slow diffusion of diethyl ether into separate solutions of $Pb_2\mathbf{1}(ClO_4)_4$ in CH_3CN and CH_3NO_2.

$Pb_2\mathbf{1}(SO_3CF_3)_4$. $Pb_2\mathbf{1}(SO_3CF_3)_4$ was prepared as described for $Pb_2\mathbf{1}(ClO_4)_4$ but using $Pb(SO_3CF_3)_2\cdot H_2O$ (35.4 mg, 0.0676 mmol) and **1** (12.8 mg, 0.0304 mmol) in CH_3CN (2 mL), which gave a yellow solution after agitation at elevated temperatures. Yellow crystals of $Pb_2\mathbf{1}(SO_3CF_3)_4$ were grown from this solution (11.4 mg, 27%). Anal. Calcd for $C_{25}H_{24}N_8O_{14}F_{12}S_4Pb_2$: C, 20.98; H, 1.69; N, 7.83. Found: C, 20.86; H, 1.86; N, 7.78. ^{1}H NMR (400 MHz, CD_3CN) δ/ppm: 8.72 (2H, s, H9), 8.22 (2H, t, J = 7.8 Hz, H12), 7.94 (2H, d, J = 7.5 Hz, H11), 7.70 (2H, d, J = 7.8 Hz, H13), 6.63 (1H, s, H5), 6.11 (2H, bs, OH), 5.33 (4H, s, H15), 3.75 (6H, s, H8), 2.85 (3H, s, H7). ESMS m/z found: 777.1285, 1283.0062. Calcd for $C_{21}H_{24}N_8O_2Pb(SO_3CF_3)^+$: 776.74. Calcd for $C_{21}H_{24}N_8O_2Pb_2(SO_3CF_3)_3^+$: 1283.0108. Selected IR (KBr) ν/cm^{-1}: 3373 (m, br, OH str), 2931 (w, C−H str), 1590 (s, py), 1550 (s, C═N str), 1489 (m, py), 1447 (m, pym), 1436 (m, py), 1388 (w, pym), 1291 (s, C−O str), 1256 (s), 1226 (s), 1160 (s), 1027 (s). Crystals suitable for X-ray determination were grown by slow diffusion of diethyl ether into a CH_3CN solution of **1** and $Pb(SO_3CF_3)_2$.

$Pb_4\mathbf{1}_4(ClO_4)_8$. $Pb_4\mathbf{1}_4(ClO_4)_8$ was prepared as described for $Pb_2\mathbf{1}(ClO_4)_4$ but using $Pb(ClO_4)_2\cdot 3H_2O$ (6.7 mg, 0.016 mmol) and **1** (6.5 mg, 0.015 mmol) in CH_3NO_2 (2 mL), which gave a yellow solution after agitation at elevated temperatures. Yellow crystals of $Pb_4\mathbf{1}_4(ClO_4)_8\cdot 4H_2O$ were grown by slow diffusion of benzene into this solution (4.6 mg, 10%). Anal. Calcd for $C_{21}H_{24}N_8O_{10}Cl_2Pb\cdot H_2O$: C, 29.86; H, 3.10; N, 13.27. Found: C, 29.62; H, 3.01; N, 12.93. ^{1}H NMR (500 MHz, CD_3CN) δ/ppm: 8.37 (2H, s, H9), 8.01 (2H, t, J = 7.8 Hz, H12), 7.81 (2H, d, J = 7.6 Hz, H11), 7.28 (2H, d, J = 7.8 Hz, H13), 6.46 (1H, s, H5), 5.31 (2H, t, J = 3.5 Hz, H16), 4.84 (2H, dd, J = 3.3, 15.6 Hz, H15a), 4.79 (2H, dd, J = 3.5, 15.6 Hz, H15b), 3.71 (6H, s, H8), 1.30 (3H, s, H7). ^{13}C NMR (500 MHz, CD_3CN) δ/ppm: 167.50 (C2), 162.41 (C4, C6), 161.41 (C14), 151.61 (C10), 141.89 (C9), 141.15 (C12), 127.67 (C11), 123.76 (C13), 87.28 (C5), 64.15 (C15), 36.03 (C8), 26.17 (C7). ESMS found m/z: 421.22531. Calcd for $C_{21}H_{24}N_8O_2^+$ m/z: 421.2095. Selected IR (KBr)/cm^{-1} ν: 3419 (m, br, OH str), 2931 (w, CH str), 1589 (s), 1551 (s, C═N str), 1497 (m), 1448 (m, br), 1296 (m), 1159 (m), 1091 (s, br), 1047 (s), 985 (m). Crystals suitable for X-ray determination were grown by slow diffusion of diethyl ether and benzene, respectively, into a CH_3CN and a CH_3NO_2 solution of $Pb_4\mathbf{1}_4(ClO_4)_8$.

$Pb_4\mathbf{1}_4(SO_3CF_3)_8$. $Pb_4\mathbf{1}_4(SO_3CF_3)_8$ was prepared as described for $Pb_2\mathbf{1}(ClO_4)_4$ but using $Pb(SO_3CF_3)\cdot H_2O$ (14.1 mg, 0.027 mol) and **1** (11.3 mg, 0.027 mol) in CH_3CN (2 mL), which gave a yellow solution after agitation at elevated temperatures. A yellow precipitate of $Pb\mathbf{1}(SO_3CF_3)_2$ was formed by diffusion of diethyl ether into this solution (15.2 mg, 61%). Anal. Calcd for $C_{21}H_{24}N_8O_2Pb(SO_3CF_3)_2$: C, 29.84; H, 2.61; N, 12.10. Found: C, 29.79; H, 2.74; N, 12.09. ^{1}H NMR (400 MHz, CD_3CN) δ/ppm: 8.37 (2H, s, H9), 7.95 (2H, t, J = 7.2 Hz, H12), 7.74 (2H, d, J = 7.2 Hz, H11), 7.3 (2H, d, J = 6.9 Hz, H13), 6.51 (1H, s, H5), 5.63 (2H, s, OH), 4.75 (2H, d, J = 13.5 Hz, H15a), 4.62 (2H, d, J = 14.6 Hz, H15b), 3.71 (6H, s, H8), 1.76 (3H, s, H7). ESMS m/z found: 1703.2138, 1197.3370, 777.1367, 627.1835, 421.2148. Calcd for $(C_{21}H_{24}N_8O_2)_2Pb_2(SO_3CF_3)_3^+$: 1703.2138. Calcd for $(C_{21}H_{24}N_8O_2)_2Pb(SO_3CF_3)^+$: 1197.3311. Calcd for $C_{21}H_{24}N_8O_2$-$Pb(SO_3CF_3)^+$: 777.1309. Calcd for $C_{21}H_{23}N_8O_2Pb^+$: 627.1710. Calcd for $C_{21}H_{25}N_8O_2^+$: 421.2100. Selected IR (KBr) ν/cm^{-1}: 3357 (w, OH str), 1587 (m), 1546 (s, C═N str), 1487 (m), 1434 (m), 1286 (s), 1221 (s), 1154 (s), 1044 (s), 1026 (s), 983 (s). Yellow crystals were repetitively grown by the slow diffusion of diethyl ether into a CH_3CN solution of $Pb_4\mathbf{1}_4(SO_3CF_3)_8$; however, none of the crystals produced a good enough diffraction pattern for the structure to be solved.

$Zn_2\mathbf{1}(SO_3CF_3)_4$. $Zn_2\mathbf{1}(SO_3CF_3)_4$ was prepared as described for $Pb_2\mathbf{1}(ClO_4)_4$ but using $Zn(SO_3CF_3)_2$ (21.5 mg, 0.059 mmol) and **1** (12.0 mg, 0.029 mmol) in CH_3CN (2 mL), which gave a yellow solution with agitation at room temperature. Yellow crystals of $Zn_2\mathbf{1}(SO_3CF_3)_4$-$(H_2O)_4(C_4H_{10}O)$ were grown by slow diffusion of diethyl ether into this solution (20.0 mg, 55%). Anal. Calcd for $C_{29}H_{42}N_8O_{19}F_{12}S_4Zn_2$: C, 26.92; H, 3.27; N, 8.66. Found: C, 27.19; H, 3.17; N, 8.74. ^{1}H NMR (400 MHz, CD_3CN) δ/ppm: 8.35 (2H, s, H9), 8.22 (2H, t, J = 7.8 Hz, H12), 7.86 (2H, d, J = 7.5 Hz, H11), 7.65 (2H, d, J = 8.0 Hz, H13), 6.79 (1H, s, H5), 6.54 (2H, t, J = 3.5 Hz, OH), 5.08 (4H, d, J = 3.7 Hz, H15), 3.79 (6H, s, H8), 2.97 (3H, s, H7). ESMS m/z found: 994.9092, 663.0736. Calcd for $C_{21}H_{24}N_8O_2Zn_2(SO_3CF_3)_3^+$: 994.9160. Calcd for $C_{21}H_{24}N_8O_2Zn(SO_3CF_3)^+$: 633.0834. Selected IR (KBr) ν/cm^{-1}: 3455 (s, br, O−H str), 3064 (m, C−H str), 1626 (m), 1597 (s), 1579 (s), 1557 (s, C═N str), 1495 (m), 1457 (m), 1433 (m), 1387 (m), 1289 (s), 1260 (s), 1160 (s), 1094 (w), 1053 (s), 1034 (s), 1008 (m). Yellow crystals suitable for X-ray determination were grown by slow diffusion of diethyl ether into a CH_3CN solution of $Zn_2\mathbf{1}(SO_3CF_3)_4$.

$Zn_2\mathbf{1}(BF_4)_4$. $Zn_2\mathbf{1}(BF_4)_4$ was prepared as described for $Pb_2\mathbf{1}$-$(ClO_4)_4$ but using $Zn(BF_4)_2\cdot H_2O$ (20.2 mg, 0.079 mmol) and **1** (14.8 mg, 0.035 mmol) in CH_3CN (2 mL), which gave a yellow solution with agitation at room temperature. Yellow crystals of $Zn_2\mathbf{1}$-$(BF_4)_4\cdot 2H_2O$ were grown by the slow diffusion of diethyl ether into this solution (13.5 mg, 43%). Anal. Calcd for $C_{21}H_{24}N_8O_2B_4F_{16}Zn_2\cdot 2H_2O$: C, 26.99; H, 3.02; N, 11.99. Found: C, 26.75; H, 3.44; N, 11.69. ^{1}H NMR (CD_3CN, 400 MHz) δ/ppm: 8.35 (2H, s, H9), 8.23 (2H, t, J = 7.8 Hz, H12), 7.87 (2H, d, J = 7.4 Hz, H11), 7.67 (2H, d, J = 7.9 Hz, H13), 6.76 (1H, s, H5), 5.83 (2H, t, J = 3.7 Hz, H17), 5.09 (4H, d, J = 3.8 Hz, H16), 3.79 (6H, s, H8), 2.89 (3H, s, H7). ESMS m/z found: 483.12808, 517.29733. Calcd for $C_{21}H_{23}N_8O_2Zn^+$: 483.12300. Calcd for $C_{21}H_{24}N_8O_2ZnBF_4^+$: 517.1342. Selected IR (KBr) ν/cm^{-1}: 3456 (s, br, OH str), 3061 (w, CH str), 1597 (s), 1557 (s, C═N str), 1496 (m), 1457 (m), 1432 (m), 1386 (w), 1294 (s), 1161 (s), 1056 (s, br). Yellow crystals suitable for X-ray determination were grown by slow diffusion of CH_2Cl_2 into a CH_3CN solution of $Zn_2\mathbf{1}(BF_4)_4$.

X-ray Crystallography. Crystallographic data are summarized in Table 1. X-ray diffraction data were collected on a Bruker APEX II CCD diffractometer, with graphite monochromated Mo Kα (λ = 0.71073 Å) radiation. Intensities were corrected for Lorentz polarization effects,[21] and a multiscan absorption correction[22] was applied. The structures were solved by direct methods (SHELXS[23] or SIR-97[24]) and refined on F^2 using all data by full-matrix least-squares procedures (SHELXL 97[25]). All calculations were performed using the WinGX interface.[26] Detailed analyses of the extended structure were carried out using PLATON[27] and MERCURY[28] (Version 1.4.1). X-ray data were deposited with the Cambridge Crystallographic Data Center CCDC 829094−829100. These data can be obtained free of charge from the Cambridge Crystallographic Data Center via www.ccdc.cam.ac.uk/data_request/cif. Some of the crystal structures contained disordered components. The bound ClO_4^- anions in $[Pb\mathbf{1}(ClO_4)]_4(ClO_4)_4$ (**5**) and $[Pb\mathbf{1}(ClO_4)]_4(ClO_4)_4\cdot$ $4CH_3NO_2$ (**6**) were disordered over two sites, with site occupancy factors of 0.51 and 0.49, and 0.58 and 0.42, respectively. $[Zn_2\mathbf{1}(BF_4)$-$(H_2O)_2(CH_3CN)](BF_4)_3\cdot H_2O$ (**8**) contained a BF_4^- anion disordered about a 3-fold axis, with site occupancy factors 0.62 and 0.38, and a hydroxymethyl arm disordered over two sites due to rotation about the C1−C2 bond, with site occupancy of 0.63 and 0.37.

RESULTS AND DISCUSSION

Synthesis and Structures of Complexes. The metal salts $Pb(ClO_4)_2\cdot 3H_2O$, $Pb(SO_3CF_3)_2\cdot H_2O$, $Zn(BF_4)_2\cdot H_2O$, and

dx.doi.org/10.1021/ic200670w |Inorg. Chem. 2011, 50, 7637–7649

Table 1

	$[Pb_2\mathbf{1}(ClO_4)_4]$ (**2**)	$[Pb_2\mathbf{1}(ClO_4)_3(H_2O)]\ ClO_4$ (**3**)	$[Pb_2\mathbf{1}(SO_3CF_3)_3(H_2O)]\cdot SO_3CF_3$ (**4**)	$[Pb\mathbf{1}(ClO_4)]_4(ClO_4)_4$ (**5**)
formula	$C_{21}H_{24}Cl_4N_8O_{18}Pb_2$	$C_{21}H_{24}Cl_4N_8O_{19}Pb_2$	$C_{25}H_{26}F_{12}N_8O_{15}Pb_2S_4$	$C_{84}H_{96}Cl_8N_{32}O_{40}Pb_4$
formula weight	1232.68	1250.68	1449.16	3306.33
crystal system	triclinic	triclinic	triclinic	tetragonal
space group	*P*-1	*P*-1	*P*-1	*I*4(1)/*a*
a/Å	9.8273(17)	9.1759(18)	10.1195(9)	27.9354(13)
b/Å	12.010(2)	11.974(2)	12.6995(11)	27.9354(13)
c/Å	15.111(3)	16.043(3)	17.7334(15)	15.2254(8)
α/deg	75.586(8)	84.705(9)	71.677(4)	90
β/deg	73.672(9)	80.236(11)	73.808(4)	90
γ/deg	76.293(8)	78.353(9)	79.069(4)	90
V/Å^3	1630.7(5)	1698.3(5)	2064.6(3)	11882(2)
Z	2	2	2	4
T/K	90(2)	90(2)	90(2)	90(2)
μ/mm^{-1}	10.733	10.309	8.476	5.924
reflections collected	23 504	30 902	25 610	74 191
unique reflections (R_{int})	6036 (0.0352)	6292 (0.0299)	7682 (0.0313)	5528 (0.0498)
R_1 indices [$I > 2\sigma(I)$]	0.0266	0.0163	0.0270	0.0402
wR2 (all data)	0.0654	0.0501	0.1106	0.1225
GOF	1.054	1.195	1.157	1.193

	$[Pb\mathbf{1}(ClO_4)]_4\ (ClO_4)_4\cdot 4CH_3NO_2$ (**6**)	$[Zn_2\mathbf{1}(H_2O)_4](SO_3CF_3)_4\cdot C_2H_5O$ (**7**)	$[Zn_2\mathbf{1}(BF_4)(H_2O)_2(CH_3CN)]\ (BF_4)_3\cdot H_2O$ (**8**)
formula	$C_{87}H_{96}Cl_8N_{35}O_{46}Pb_4$	$C_{29}H_{42}F_{12}N_8O_{19}S_4Zn_2$	$C_{23}H_{31}B_4F_{16}N_9O_5Zn_2$
formula weight	3480.00	1293.69	991.55
crystal system	tetragonal	triclinic	triclinic
space group	*I*4(1)/*a*	*P*-1	*P*-1
a/Å	27.861(4)	13.5655(13)	7.6091(7)
b/Å	27.861(4)	14.274(3)	14.2283(15)
c/Å	15.258(4)	14.2890(15)	18.693(2)
α/deg	90	101.348(7)	111.154(4)
β/deg	90	113.591(5)	91.646(4)
γ/deg	90	98.629(7)	102.494(4)
V/Å^3	11844(4)	2404.2(6)	1829.9(3)
Z	4	2	2
T/K	90(2)	90(2)	90(2)
μ/mm^{-1}	5.953	1.298	1.442
reflections collected	70 437	44 299	19 047
unique reflections (R_{int})	5508 (0.0452)	8953 (0.0340)	5728 (0.0411)
R_1 indices [$I > 2\sigma(I)$]	0.0451	0.0260	0.0845
wR2 (all data)	0.1003	0.0982	0.2286
GOF	1.208	1.218	1.047

$Zn(SO_3CF_3)_2$ were dissolved in CH_3CN or CH_3NO_2 and added to ligand **1** in a 2:1 molar ratio to yield yellow solutions of the 2:1 complexes. CD_3CN was used to make solutions of the 2:1 complexes for analysis by NMR spectroscopy. Diffusion of a nonsolvent into the complex solutions yielded yellow solid materials, which were dried in vacuo, then analyzed by microanalysis, mass spectroscopy, and infrared spectroscopy. The microanalytical results of these complexes were consistent with a 2:1 metal-to-ligand ratio. Some of the complexes, $Pb\mathbf{1}(ClO_4)_2\cdot 4H_2O$, $Zn_2\mathbf{1}(BF_4)_4\cdot 2H_2O$, and $Zn_2\mathbf{1}(SO_3CF_3)_4\cdot 4H_2O\cdot C_5H_{10}O$, were solvated despite prolonged drying under high vacuum.

$Pb(ClO_4)_2\cdot 3H_2O$ was also reacted with **1** in a 1:1 molar ratio in CH_3CN and CH_3NO_2 to form yellow solutions of the 1:1 complex. This reaction was repeated in CD_3CN for NMR studies. Slow diffusion of a nonsolvent yielded yellow crystals. The microanalytical results from these crystals were consistent with the empirical formula of $Pb\mathbf{1}(ClO_4)_2\cdot H_2O$. $Pb(SO_3CF_3)_2\cdot H_2O$ was also reacted with **1** in a 1:1 molar ratio in CH_3CN. Diffusion of diethyl ether into the yellow solution resulted in a yellow solid, which provided microanalytical results consistent with the empirical formula $Pb\mathbf{1}(SO_3CF_3)_2$. The reaction was repeated in CD_3CN for NMR studies.

No complexes were obtained from reacting $Zn(SO_3CF_3)_2$ and $Zn(BF_4)_2\cdot H_2O$ in a 1:1 ratio with **1**. Addition of the Zn(II) salts in CH_3CN to a stirring, heated suspension of **1** in CH_3CN resulted in instantaneous dissolution of **1**, forming yellow solutions. A light precipitate of **1** would then emerge from the

dx.doi.org/10.1021/ic200670w |*Inorg. Chem.* 2011, 50, 7637–7649

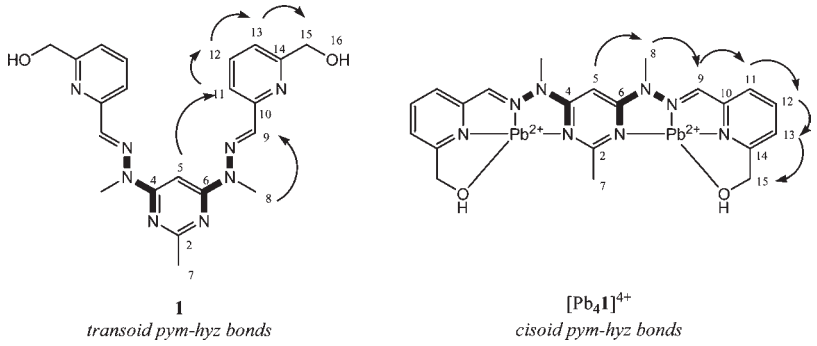

1
transoid pym-hyz bonds

$[Pb_2\mathbf{1}]^{4+}$
cisoid pym-hyz bonds

Figure 1. (left) Structure of the free ligand **1**, showing its NOE correlations, which demonstrate its horseshoe shape. The transoid pym−hyz bonds are highlighted. (right) Structure of the $[Pb_2\mathbf{1}]^{4+}$ cation common to $Pb_2\mathbf{1}(ClO_4)_4$ and $Pb_2\mathbf{1}(SO_3CF_3)_4$, showing the NOE correlations, which allude to the linear structure of the complexes. The cisoid pym−hyz bonds are highlighted (showing NMR numbering).

solutions at room temperature. ^{1}H NMR spectra of the reactions in CD_3CN showed a set of significantly broadened peaks with chemical shifts similar to those seen for **1**.[11] It appeared that the Zn(II) ions merely caused dissolution of **1** and that any complex formation was short-lived.

NMR Spectroscopy. The ^{1}H NMR spectra of the $Pb_2\mathbf{1}(ClO_4)_4$ and $Pb_2\mathbf{1}(SO_3CF_3)_4$ complexes in CD_3CN were identical, suggesting that the ClO_4^- or $SO_3CF_3^-$ anions were labile in solution. Both spectra showed only nine peaks, indicating a symmetric complex arising from Pb(II) ions occupying both coordination sites of **1**. The rotation of the pym−hyz linkages from the transoid conformation in **1** to the cisoid conformation in the 2:1 Pb(II) complexes resulted in a linear shape as evidenced by the presence of NOE correlations between $H5_{pym}$, $H8_{hyz}$, $H9_{hyz}$, and $H11_{py}$, while there was no correlation between $H5_{pym}$ and $H11_{py}$. This contrasts with the free ligand **1**, which showed NOE correlations between $H5_{pym}$ and $H11_{hyz}$, with no correlation between $H5_{pym}$ and $H8_{hyz}$ (Figure 1).[11]

Coordination of the Pb(II) ions to **1** resulted in a downfield shift of the hyz and py protons as compared to the free ligand. This was most noticeable for $H9_{hyz}$, which shifted from 7.87 ppm in **1** to 8.73 ppm in $Pb_2\mathbf{1}(ClO_4)_4$, and the hydroxymethyl arm protons H15 and H16, which were downshifted from 4.63 and 5.37 ppm to 5.34 and 6.11 ppm, respectively.[11] These shifts were indicative of the coordination of the pym−hyz−py N donors and the hydroxymethyl arms to the Pb(II) ions. In contrast, the pyrimidine $H5_{pym}$ peak was shifted upfield from 7.65 ppm in **1** to 6.65 ppm in $Pb_2\mathbf{1}(ClO_4)_4$, possibly due to the change in shape of the pym−hyz bonds (Figure 2).[11]

The ^{1}H NMR spectrum of the 1:1 $Pb(ClO_4)_2$ complex suggested the ligand and Pb(II) ions formed a $[2 \times 2]$ square grid in solution. The number of signals in the 1:1 complex spectrum was the same as the 2:1 complex spectra, which suggested a Pb(II) ion occupied each of the ligands' pym−hyz−py sites. NOE correlations existed between $H5_{pym}$, $H8_{hyz}$, and $H9_{hyz}$ due to both pym−hyz linkages in the 1:1 complex adopting a cisoid conformation. The signal due to the H15 methylene protons showed germinal coupling, as a result of the protons being in different chemical environments, as one of the methylene protons was orientated toward one of the other ligands of the grid, while the other pointed out away from the grid. Rotation of the hydroxymethyl arm was restricted as a a result of the coordination of the OH groups to the Pb(II) ions. The strong shielding of the H7 methyl protons suggested that these protons pointed into the center of the grid (Figure 2). The 1:1 $Pb(SO_3CF_3)_2$ complex ^{1}H NMR spectrum was similar, with only slight changes in chemical shift for the aromatic and methylene protons. The H7 methyl proton signal was located at 1.76 ppm, while in the 1:1 $Pb(ClO_4)_2$ complex this signal appeared at 1.30 ppm, and in the 2:1 Pb(II) complexes it was at 2.85 ppm.

The spectra of the 2:1 Zn(II)/**1** complexes were similar to those of the 2:1 Pb(II)/**1** complexes. Both spectra showed eight peaks, which suggested a Zn(II) ion occupied each coordination pocket. The signals from the hyz, py, and hydroxymethyl protons were downshifted relative to **1**, which indicated that the three pym−hyz−py N donors and the hydroxymethyl O donor were coordinated to the Zn(II) ions. These shifts were of a smaller magnitude than those seen in the 2:1 Pb(II)/**1** complexes. The $H5_{pym}$ signal was also upshifted as a result of the linear shape of the complex, but by a smaller amount than that seen in the 2:1 Pb(II)/**1** complexes.

^{1}H NMR spectroscopy was also used to monitor the 2:1 Zn(II)/**1** complex solution as it was treated with an increasing amount of $Pb(SO_3CF_3)_2 \cdot H_2O$. The complexes present were identified by focusing on the aromatic region of the ^{1}H NMR spectra (Figure 3). As the molar equivalence of Pb(II) ions was increased, the peaks due to the $Zn_2\mathbf{1}(SO_3CF_3)_4$ complex decreased in intensity, as new peaks due to the $Pb_2\mathbf{1}(SO_3CF_3)_4$ complex and a new linear heterometallic $ZnPb\mathbf{1}(SO_3CF_3)_4$ complex arose. The heterometallic complex was the most abundant complex as the Pb(II) ions were increased from a molar equivalence of 0.5 to 2.0. At 2.0, there was an equal amount of the heterometallic and the $Pb_2\mathbf{1}(SO_3CF_3)_4$ complexes, with a trace amount of the $Zn_2\mathbf{1}(SO_3CF_3)_4$. By 3.0 equivalence of Pb(II) ions, all of the $Zn_2\mathbf{1}(SO_3CF_3)_4$ had been converted into the heterometallic and the $Pb_2\mathbf{1}(SO_3CF_3)_4$, which existed at a molar ratio of 4:5. Once a 5.0 molar equivalence of Pb(II) ions had been added, this molar ratio was 1:4.

The titration of $Pb_2\mathbf{1}(SO_3CF_3)_4$ with $Zn(SO_3CF_3)_2$ produced complementary results, with the $Pb_2\mathbf{1}(SO_3CF_3)_4$ complex undergoing metal ion exchange to form the $PbZn\mathbf{1}(SO_3CF_3)_4$ and $Zn_2\mathbf{1}(SO_3CF_3)_4$ complexes. Addition of $Zn(SO_3CF_3)_2$ to the 1:1 $Pb(SO_3CF_3)_2$/**1** complex also resulted in a mixture of the three complexes seen in Figure 3. This mixture was also achieved when solutions of $Pb_2\mathbf{1}(SO_3CF_3)_4$ and $Zn_2\mathbf{1}(SO_3CF_3)_4$ were combined. Attempts to synthesize the heterometallic complex by reacting **1** with $Pb(SO_3CF_3)_4$ and $Zn(SO_3CF_3)_4$ in a 1:1:1 molar ratio also gave a mixture of the three complexes. These results demonstrate the labile nature of the Pb(II) and Zn(II) ions in the complexes of **1**, as they freely exchange between complexes.

dx.doi.org/10.1021/ic200670w |*Inorg. Chem.* 2011, 50, 7637–7649

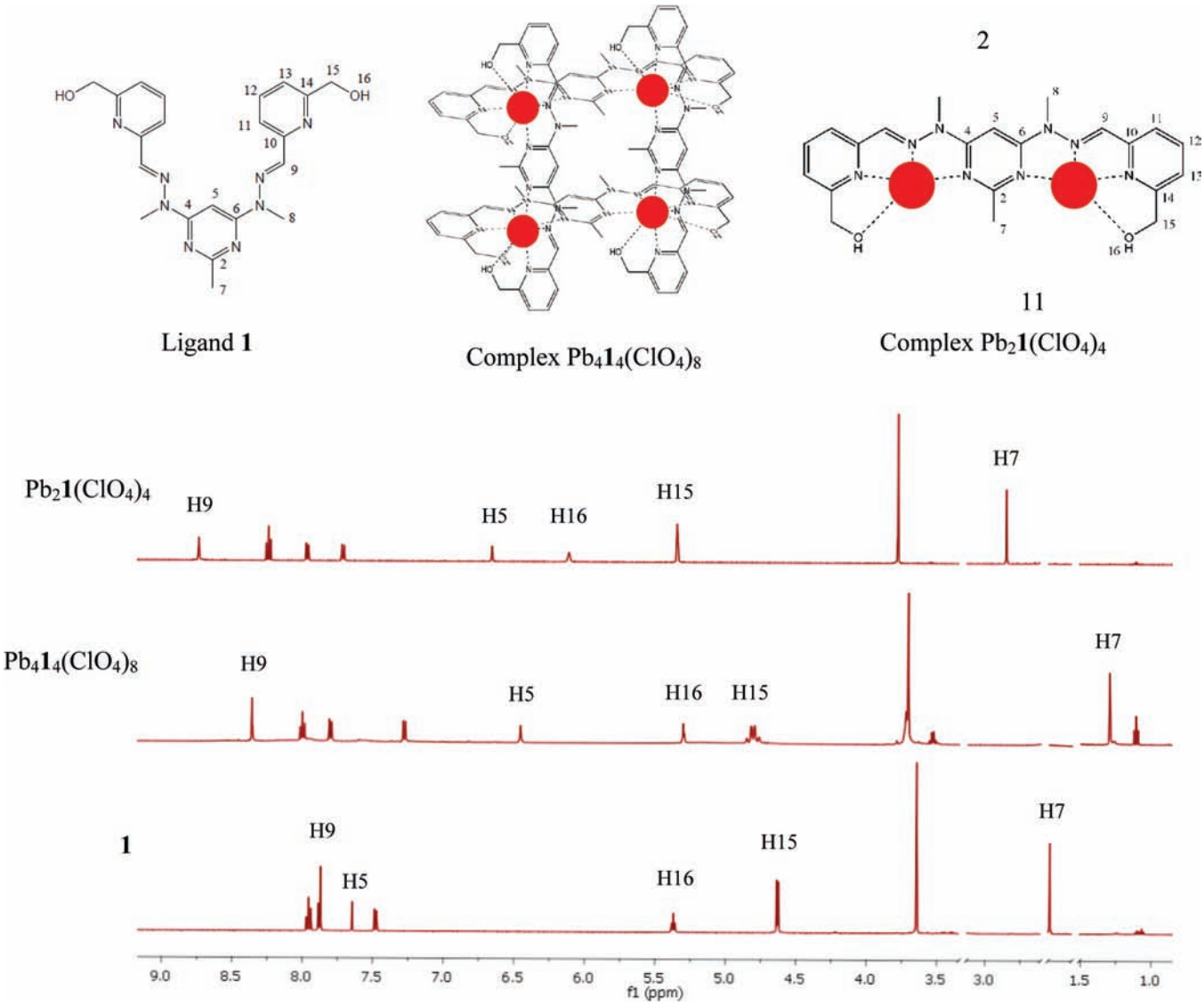

Figure 2. Structures and ^{1}H NMR spectra of the ligand **1**, and the 1:1 and 2:1 metal/ligand complexes made from **1** and $Pb(ClO_4)_2 \cdot 3H_2O$. The free ligand has both pym−hyz bonds in their transoid conformation, while both of these bonds are cisoid in the two complexes (NMR numbering; signals due to solvent and H_2O are omitted for clarity).

Electrospray Mass Spectroscopy. Both 2:1 Pb(II) complexes $Pb_2\mathbf{1}(ClO_4)_4$ and $Pb_2\mathbf{1}(SO_3CF_3)_4$ lost a Pb(II) ion to form the molecular ions $[Pb\mathbf{1} - H]^+$ and $[Pb\mathbf{1}(SO_3CF_3)]^+$, respectively. The $Zn_2\mathbf{1}(BF_4)_4 \cdot 2H_2O$ complex similarly formed the $[Zn\mathbf{1} - H]^+$ fragment, while the $Zn_2\mathbf{1}(SO_3CF_3)_2 \cdot 4H_2O \cdot C_5H_{10}O$ complex retained both Zn(II) ions to form a $[Zn_2\mathbf{1}(SO_3CF_3)_3]^+$ molecular ion. The $Pb_4\mathbf{1}_4(ClO_4)_8$ grid complex disassembled during ionization, resulting in a base peak corresponding to the molecular ion $[\mathbf{1} + H]^+$. The ESMS spectrum of the $Pb_4\mathbf{1}_4(SO_3CF_3)_8$ grid complex, on the other hand, showed several peaks due to fragments of the $[2 \times 2]$ grid. These fragments were $[Pb_2\mathbf{1}_2(SO_3CF_3)_3]^+$, $[Pb\mathbf{1}_2(SO_3CF_3)]^+$, $[Pb\mathbf{1}(SO_3CF_3)]^+$, and $[Pb\mathbf{1} - H]^+$.

Infrared Spectroscopy. The IR spectra of the three Pb(II) complexes all showed a decrease in frequency for the C═N stretch relative to the free ligand **1** of roughly 10 cm^{-1}. The 2:1 and 1:1 Pb(II) structures all showed very similar spectra, with the only difference being the increase in number of bands from 1291 to 1226 cm^{-1} in the $Pb_2\mathbf{1}(SO_3CF_3)_4$ and $Pb_4\mathbf{1}_4(SO_3CF_3)_4$ spectra due to the $SO_3CF_3^-$ ions. The 2:1 Zn(II) complexes exhibited intense stretching bands at 1598 and 1579 cm^{-1}, in addition to the C═N stretching mode at 1557 cm^{-1}. All of the complexes showed an increase in frequency of the OH stretching band relative to the free ligand **1**, due to coordination of the hydroxymethyl arm to the Pb(II) or Zn(II) ions.

X-ray Crystallography. X-ray quality crystals were grown by the slow diffusion of nonsolvents diethyl ether, benzene, or CH_2Cl_2 into CH_3CN or CH_3NO_2 solutions of the 2:1 and 1:1 metal/ligand mixtures. All of the crystals grown were yellow in color. Analysis of these crystals by single crystal X-ray diffraction yielded the structures **2**−**8**.

Single crystals were repetitively grown of the 1:1 $Pb(SO_3CF_3)_2$/**1** complex through slow diffusion of diethyl ether into the $Pb_4\mathbf{1}_4(SO_3CF_3)_8$ solution. Several of these crystals were analyzed by X-ray diffraction; however, none of the crystals produced a diffraction pattern good enough to allow elucidation of their solid-state structure.

dx.doi.org/10.1021/ic200670w |*Inorg. Chem.* 2011, 50, 7637–7649

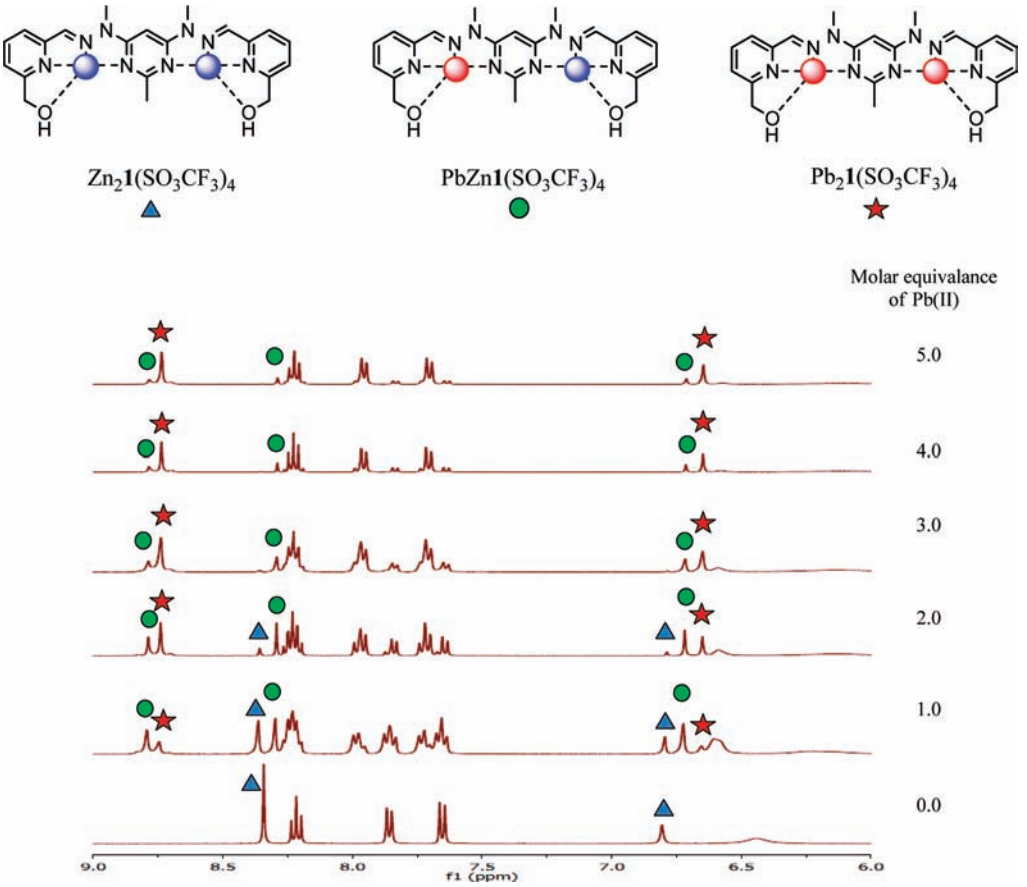

Figure 3. ^{1}H NMR spectra following the titration of the 2:1 Zn(II)/**1** complex (bottom) with $Pb(SO_3CF_3)_2.H_2O$ from a 0.5 to a 5.0 molar equivalence. The H_{hyz} and $C5_{pym}$ peaks for the $Zn_2\mathbf{1}(SO_3CF_3)_4$ (blue ▲), the heterometallic $PbZn\mathbf{1}(SO_3CF_3)_4$ (green ●), and the $Pb_2\mathbf{1}(SO_3CF_3)_4$ (red ★) complexes are labeled.

X-ray Structure of $[Pb_2\mathbf{1}(ClO_4)_4]$ 2. Complex **2** was crystallized by the slow diffusion of diethyl ether into a 2:1 mixture of $Pb(ClO_4)_2\cdot 3H_2O$ and **1** in CH_3CN. The complex crystallized in the triclinic space group *P*-1 with one complete complex moiety in the asymmetric unit. The complex had a linear shape, with both pym−hyz bonds adopting a cisoid conformation (Figure 4). The distance between the centroids of the terminal pyridine rings was 14.10 Å, which was significantly longer than the equivalent distance of 6.73 Å measured previously across the free ligand **1**.[11] It is also longer than the distances of 12.59 and 12.67 Å, which were measured across the dicopper complexes $[Cu_2\mathbf{1}(CH_3CN)_4](ClO_4)\cdot CH_3CN$ and $[Cu_2\mathbf{1}(SO_3CF_3)_2(CH_3CN)_2](SO_3CF_3)_2\cdot CH_3CN$, respectively.[11]

Each Pb(II) ion was in a six coordinate environment, which resembled a distorted pentagonal bipyramid with the three N atoms and one O atom of each pym−hyz−py site occupying the equatorial sites and two ClO_4^- ions coordinated in axial positions (Figure 4). The large O1−Pb1−N4 and O2−Pb2−N5 angles of 155.52(16)° and 169.77(16)°, respectively, suggested the presence of a stereochemically active lone pair of electrons occupying the remaining equatorial coordination sites on Pb1 and Pb2.

Molecules of **2** were organized into dimers by two pairs of self-complementary H-bonding interactions between two of the coordinated ClO_4^- anions on one molecule and both of the hydroxymethyl arms on a neighboring molecule. The O1−H1···O42 and O2−H2···O22 distances were 1.995(4) and 1.937(4) Å, respectively [corresponding to O1···O42 and O2···O22 distances of 2.782(5) and 2.685(6) Å, respectively]. These dimers were then arranged into a one-dimensional chain, running in the [100] direction, by a self-complementary anion−π interaction between the central pyrimidine ring of a dimer and one of the ClO_4^- anions of an adjacent dimer (Figure 5). The distance from the centroid of the pyrimidine ring to the ClO_4^- atom O44 was 3.1234(6) Å.

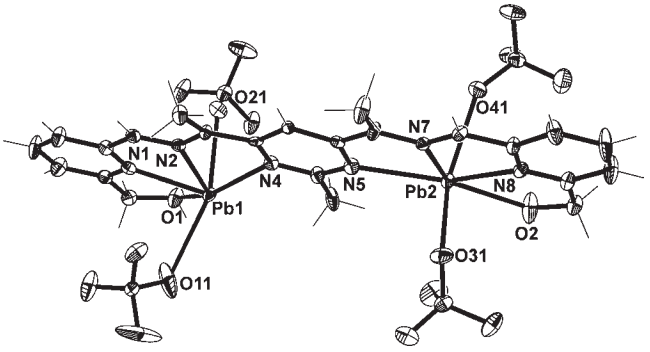

Figure 4. View of complex **2** (crystallographic numbering). Thermal ellipsoids drawn at the 50% probability level.

X-ray Structure of $[Pb_2\mathbf{1}(ClO_4)_3(H_2O)](ClO_4)$ 3. Complex **3** was crystallized from the slow diffusion of diethyl ether into a 2:1 mixture of $Pb(ClO_4)_2\cdot 3H_2O$ and **1** dissolved in CH_3NO_2. The

dx.doi.org/10.1021/ic200670w |*Inorg. Chem.* 2011, 50, 7637–7649

complex crystallized in the triclinic space group *P*-1 with one complete cation $[Pb_2\mathbf{1}(ClO_4)_3(H_2O)]^+$ and a ClO_4^- counterion in the asymmetric unit. As with complex **2**, complex **3** was a planar, linear complex, with a centroid-to-centroid distance of 14.08 Å between the terminal pyridine rings. Each Pb(II) ion was in a distorted six-coordinate, pentagonal bipyramid environment,

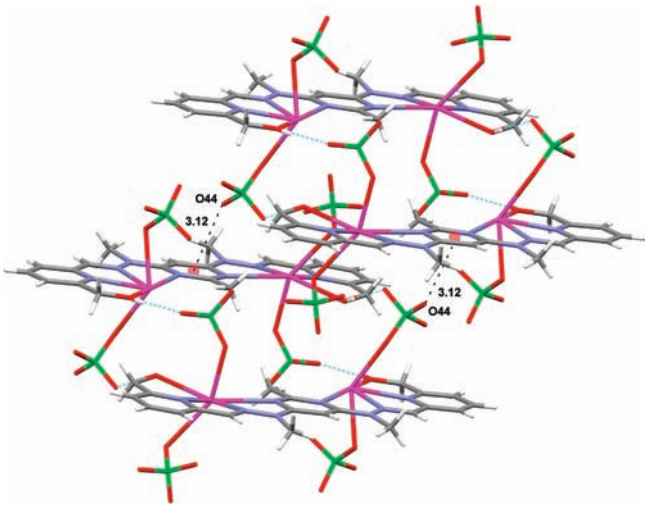

Figure 5. View of a pair of dimers of **2** showing the interdimer anion−π interaction between the pyrimidine ring on one dimer and the O44 atom of a ClO_4^- anion on the other dimer. Also shown are the intradimer self-complementary H-bonding interactions between the hydroxymethyl arms and the ClO_4^- anions.

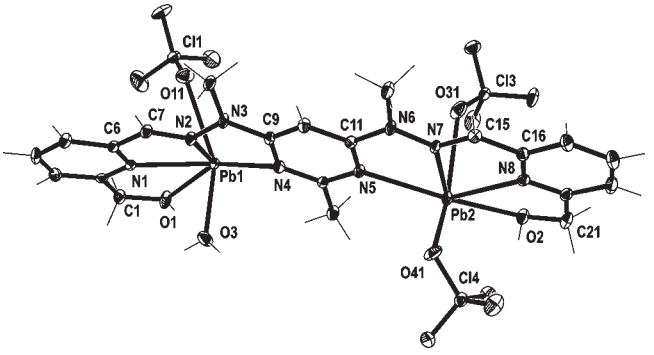

Figure 6. View of the $[Pb_2\mathbf{1}(H_2O)(ClO_4)_3]^+$ cation of complex **3** (crystallographic numbering). Thermal ellipsoids drawn at the 50% probability level.

with the three N donors and the O donor of the pym−hyz pocket occupying the equatorial positions of the Pb coordination spheres. The $N4_{pym}$ and $N5_{pym}$ donor distances to Pb1 and Pb2 were somewhat long at 2.819(3) and 2.706(3) Å, respectively; however, a search of Pb(II)−N bond lengths using the Cambridge Structural Database (CSD version 5.29)[29] revealed that they were of an acceptable length for a Pb−N bond (2004 bond distances in 647 complexes, range from 2.08 to 3.23 Å). The large N4−Pb1−O1 and O2−Pb2−N5 angles of 152.39(10)° and 167.17(9)°, respectively, were indicative of a stereochemically active lone pair on Pb1 and Pb2 occupying an equatorial site. The coordination sphere of Pb1 was completed by a ClO_4^- anion and a H_2O molecule, while Pb2 was instead coordinated to two ClO_4^- anions (Figure 6).

The free ClO_4^- anion was H-bonded to a hydroxymethyl arm of the $[Pb_2\mathbf{1}(H_2O)(ClO_4)_3]^+$ cation with a O2−H2···O24 distance of 2.760(3) Å [corresponding to an O2···O24 separation of 3.027(4) Å]. This H-bond held the ClO_4^- counteranion between the coordinated ClO_4^- anions on the same face of the mean plane as Pb1 and Pb2. The complex was organized into stepped dimers through H-bonds between the hydroxymethyl arms of one complex molecule and two of the bound ClO_4^- anions on another complex molecule (Figure 7). The O1−H1···O32 and O2−H2···O14 distances were 2.053(3) and 1.971(4) Å, respectively [corresponding to O1···O32 and O2···O14 separations of 2.782(4) and 2.754(5) Å, respectively]. The dimers were linked together through H-bonding between the H_2O molecule coordinated to Pb1 on one dimer and both the free ClO_4^- counteranion and the ClO_4^- anion bound to Pb2 of another dimer. The O3−H3···O23 distance was 2.06(6) Å [O3···O23 separation of 2.762(5) Å], and the O3−H3···O33 distance was 2.05(6) Å [O3···O33 separation of 2.785(4) Å]. The dimers formed a one-dimensional chain in the diagonal [101] direction (Figure 7).

X-ray Structure of $[Pb_2\mathbf{1}(SO_3CF_3)_3(H_2O)]\cdot SO_3CF_3$ 4. Complex **4** was crystallized by the slow addition of diethyl ether into a 2:1 mixture of $Pb(SO_3CF_3)_2\cdot H_2O$ in CH_3CN. The complex crystallized in the triclinic space group *P*-1 with one $[Pb_2\mathbf{1}(SO_3CF_3)_2(H_2O)]^{2+}$ cation and two $SO_3CF_3^-$ counterions in the asymmetric unit. The complex had a linear shape, with both pym−hyz linkages in a cisoid conformation, and a distance of 14.08 Å between the centroids of the terminal pyridine rings. Pb1 was present in a seven coordinate environment, with bonds between the OH arm and three N donors of the pym−hyz site, in addition to two $SO_3CF_3^-$ anions and a water molecule. Pb2 was present in a six coordinate, distorted pentagonal bipyramid environment, which included all three N donors and the terminal

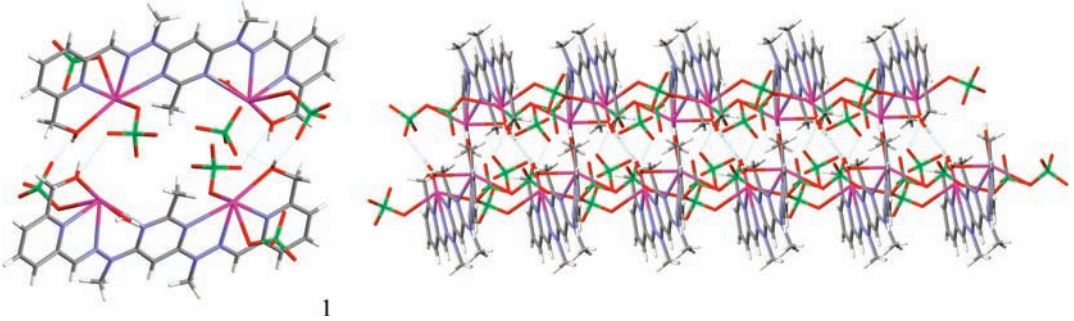

Figure 7. (left) View of the organization of **3** into a stepped dimer (one ClO_4^- counteranion has been omitted for clarity). (right) View of the assembly of the **3** dimers into a one-dimensional double chain in the diagonal [101] direction through H-bonding.

dx.doi.org/10.1021/ic200670w |*Inorg. Chem.* 2011, 50, 7637–7649

OH arm, as well as a $SO_3CF_3^-$ anion, with a stereochemically active lone pair resulting in the large N5—Pb2—O2 angle of 164.76° (Figure 8). The $SO_3CF_3^-$ anion coordinated to Pb2 bridged adjacent molecules of complex **4**, resulting in a coordination polymer running along the *a* axis (Figure 9).

Two strands of the coordination polymer were interdigitated as a result of H-bonding between the O42 on the S4 containing $SO_3CF_3^-$ anion bound to Pb1 on one polymer strand, and the H_2O molecule coordinated to Pb1 on a neighboring strand. The distance of this O3—H3A···O42 bond was 1.86(5) Å (corresponding to an O3···O42 distance of 2.737(7) Å). The S4 containing $SO_3CF_3^-$ anion was also H-bonded to O1 with a O1—H1···O43 distance of 2.30(7) Å (corresponding to O1···O43 distance of 2.798(7) Å). The uncoordinated $SO_3CF_3^-$ was H-bonded to O2 and O3 on adjacent polymer strands with O2—H2···O32 and O3—H3B···O33 distances of 2.22(7) and 1.86(3) Å, respectively (corresponding to O2···O32 and O3···O33 distances of 2.798(7) and 2.720(7) Å, respectively) (Figure 9).

X-ray Structure of $[Pb1(ClO_4)]_4(ClO_4)_4$ 5 and $[Pb1(ClO_4)]_4(ClO_4)_4\cdot 4CH_3NO_2$ 6. Complex **5** was crystallized from the slow addition of diethyl ether to a 1:1 mixture of $Pb(ClO_4)_2\cdot 3H_2O$ and **1** dissolved in CH_3CN. The complex crystallized in the tetragonal space group $I4_1/a$ with one complete $[Pb\mathbf{1}(ClO_4)]^+$ cationic motiety (Figure 10) and a ClO_4^- counterion in the asymmetric unit. Both pym—hyz linkages were in a cisoid conformation, and the centroid-to-centroid distance between the pyridine rings of the ligand backbone was 13.92 Å. Four symmetry related $[Pb\mathbf{1}(ClO_4)]^+$ cations, generated by a $\bar{4}$ special position, formed a [2 × 2] square grid, where each Pb(II) ion was shared by two ligand molecules (Figure 11). The Pb(II) ions adopted an eight coordinate, distorted trifacially capped trigonal prismatic coordination geometry, with coordination bonds formed from the 3 N donors and the hydroxymethyl O donor of a pym—hyz—py site, the O donor of a ClO_4^- anion, and bonds to O2, N7, and N8 of a pym—hyz—py site on a symmetry generated $[Pb\mathbf{1}(ClO_4)]^+$. A stereochemically lone pair existed on the Pb(II) ion resulting in the large O11—Pb1—N4 angle of 131.4(4)° (Figure 10).

The ligand backbone was twisted about the N7—C15 imine bond such that the N1 and N8 containing pyridine rings intersected the mean plane of the central pyrimidine ring at angles of 9.88° and 40.58°, respectively. As a result, individual grids of **5** were heavily distorted. The $[Pb\mathbf{1}(ClO_4)]_4(ClO_4)_4$ structure is only recognizably a grid structure when viewed down the 4-fold axis of improper rotation, which ran through the unit

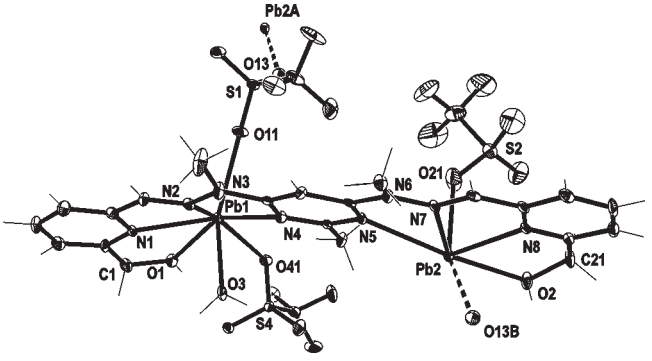

Figure 8. View of the $[Pb_2\mathbf{1}(SO_3CF_3)_3(H_2O)]^+$ cation of complex **4** (crystallographic numbering). Thermal ellipsoids drawn at the 50% probability level (symmetry codes: A, −1 + *x*, *y*, *z*; B, 1 + *x*, *y*, *z*).

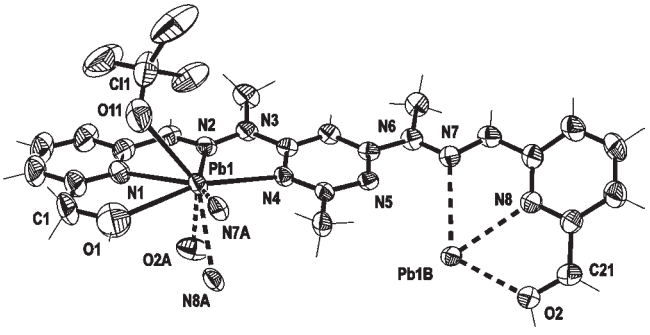

Figure 10. View of $[Pb\mathbf{1}(ClO_4)]^+$ moiety of complex **5** showing the coordination environment about the Pb(II) ion (crystallographic numbering). Thermal ellipsoids drawn at the 50% probability level (symmetry code: A, 1/4 + *x*, 5/4 − *y*, 1/4 − *z*; B, 1.25 − *x*, −1/4 + *y*, 1/4 − *z*).

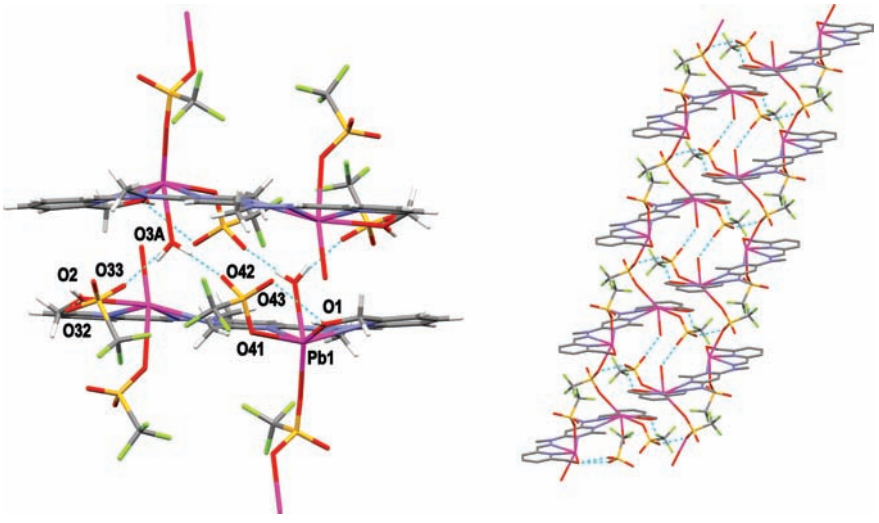

Figure 9. (left) H-bonding interactions between two adjacent cations of the interdigitated polymer strands of **4** (symmetry codes: A, −*x*, −*y*, 2 − *z*). (right) View of the two interdigitated polymer strands of **4** (hydrogens and uncoordinated $SO_3CF_3^-$ counteranions have been omitted for clarity).

dx.doi.org/10.1021/ic200670w |*Inorg. Chem.* 2011, 50, 7637–7649

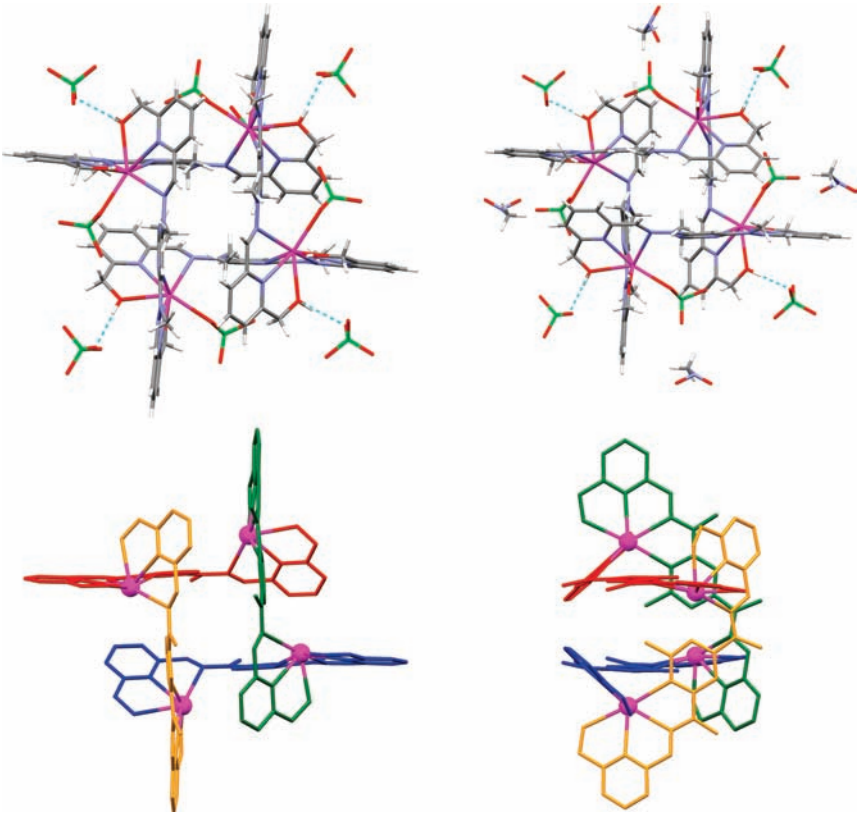

Figure 11. (top left) View of the symmetry generated [2 × 2] grid of **5**. (top right) View of the symmetry generated [2 × 2] grid of **6**. (bottom left and right) Representations of grid **5**, with the symmetrically related ligands color coded (anions and hydrogens are omitted for clarity).

cell in the [001] direction. There was a striking lack of coplanity between the four Pb(II) ions, illustrated by the separation of 3.6 Å between the centroids of the diagonal Pb−Pb distances. This twist in the ligand backbone was caused by the hydroxymethyl arms crowding the Pb(II) coordination sphere. [2 × 2] grids made with pym−hyz strands not containing coordinating groups on the terminal pyridine rings have consistently been square in shape;[2,13,15,18,19] therefore, the distorted shape of complex **5** is very unusual (Figure 11).

The hydroxymethyl arms also participated in H-bonding to the unbound ClO_4^- anions, with a O1−H···O21 distance of 2.024(6) Å [corresponding to an O1···O21 separation of 2.812(11) Å]. Another H-bond between the unbound ClO_4^- anions and the hydroxymethyl arms linked the [2 × 2] grid units together to form a three-dimensional supramolecular structure. The O2−H···O23 distance was measured as 2.241(6) Å [corresponding to an O2···O23 distance of 2.845(9) Å].

Crystals of the same morphology were also grown by the diffusion of benzene into an CH_3NO_2 solution of a 1:1 mixture of $Pb(ClO_4)_2 \cdot 3H_2O$ and **1**. The resulting complex **6** was isomorphous with **5** and had the same very distorted [2 × 2] grid structure and similar bond distances and angles (Figure 11). The only difference between the two structures was the inclusion of a CH_3NO_2 molecule of crystallization in the asymmetric unit in **6** in the interstitial spaces between the grids.

X-ray Structure of $[Zn_2\mathbf{1}(H_2O)_4](SO_3CF_3)_4 \cdot C_4H_{10}O$ 7. Complex **7** was crystallized from the slow diffusion of diethyl ether into a 2:1 mixture of $Zn(SO_3CF_3)_2$ and **1** dissolved in CH_3CN. The complex crystallized in the triclinic space group *P*-1 with one $[Zn_2\mathbf{1}(H_2O)_4]^{4+}$ cation, four $SO_3CF_3^-$ counterions, and a diethyl ether molecule of crystallization in the asymmetric unit. The complex had a linear shape, with both pym−hyz linkages in a cisoid conformation, analogous to the other linear complexes **2**−**4** (Figure 12). The centroid-to-centroid distance between the terminal pyridine rings of **7** was shorter than those of complexes **2**−**4** at 12.87 Å. This is due to **7** having a significantly bowed shape such that the planes of the N1 and N8 containing pyridine rings intersected the mean plane of the central pyrimidine ring at angles of 13.37° and 17.50° . Both of the Zn(II) ions had a distorted octahedral coordination sphere, with the three N donors of the pym−hyz pocket and the O donor of the hydroxymethyl arm in the equatorial sites and a water molecule occupying each axial site (Figure 12).

The $SO_3CF_3^-$ counterions were arranged around the $[Zn_2\mathbf{1}(H_2O)_4]^{4+}$ cation through an elegant network of H-bonds involving the H_2O molecules coordinated to Zn1 and Zn2. The S1 and S2 containing $SO_3CF_3^-$ counterions were located above and below the central pyrimidine ring, with H-bonds between O3−H3B···O11 and O5−H5A···O13 of 1.99(4) and 1.92(4) Å, respectively (corresponding to O3···O11 and O5···O13 distances of 2.717(3) and 2.749(3) Å, respectively), and O4−H4B···O22 and O6−H6B−O23 of 1.92(4) and 1.94(4) Å, respectively (corresponding to O4···O22 and O6···O23 distances of 2.723(3) and 2.730(3) Å, respectively). The S3 and S4 containing $SO_3CF_3^-$ counterions flanked the S2 containing $SO_3CF_3^-$ counterion and were H-bonded to the other hydrogen on O4 and O6 with O4−H4A···O33 and O6−H6B···O41 distances of 2.01(4) and 2.02(4) Å, respectively (corresponding to O4···O33 and O6···O41 distances of 2.742(3) and 2.788(3) Å) (Figure 13)

dx.doi.org/10.1021/ic200670w |*Inorg. Chem.* 2011, 50, 7637–7649

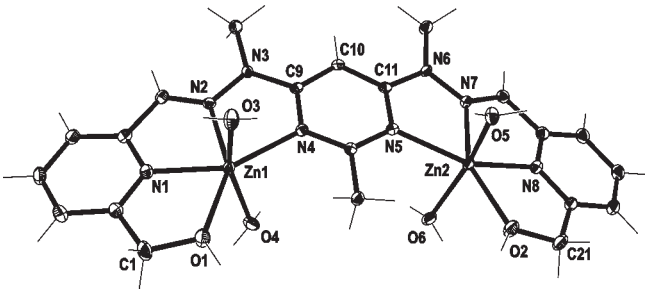

Figure 12. View of the $[Zn_2\mathbf{1}(H_2O)_4]^{4+}$ cation of complex **7** (crystallographic numbering). Thermal ellipsoids drawn at the 50% probability level.

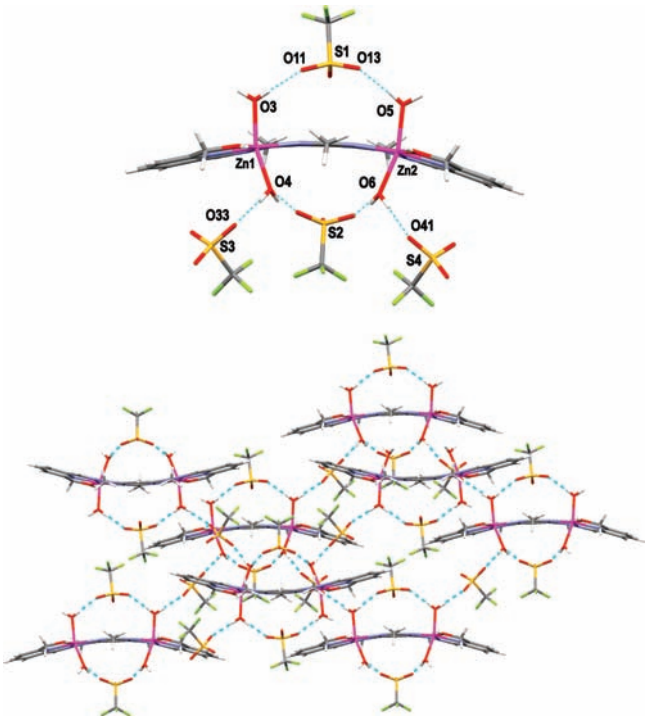

Figure 13. (top) View of the H-bonding pattern, which holds the four $SO_3CF_3^-$ counterions around the $[Zn_2\mathbf{1}(H_2O)_4]^{4+}$ cation of complex **7**. (bottom) View of the 2D sheet arrangement of $[Zn_2\mathbf{1}(H_2O)_4]^{4+}$ cations formed due to additional H-bonding between $SO_3CF_3^-$ counterions, and coordinated H_2O molecules and hydroxymethyl arms on neighboring cations.

Further H-bonding between the S3 and S4 containing $SO_3CF_3^-$ counterions and the O1 hydroxymethyl donor and coordinated H_2O molecules on neighboring $[Zn_2\mathbf{1}(H_2O)_4]^{4+}$ cations resulted in an extended 2D sheet formation (Figure 13). Additionally, the $C_4H_{10}O$ molecule was H-bonded to O2, with a O2−H···O7 distance of 1.82(5) Å (corresponding to an O2···O7 distance of 2.629(3) Å).

X-ray Structure of $[Zn_2\mathbf{1}(BF_4)(CH_3CN)(H_2O)_2](BF_4)_3(H_2O)$ 8. Complex **8** was crystallized from the slow diffusion of CH_2Cl_2 into a 2:1 mixture of $Zn(BF_4)_2$ and **1** dissolved in CH_3CN. The complex crystallized in the triclinic space group *P*-1, with one $[Zn_2\mathbf{1}(BF_4)(CH_3CN)(H_2O)_2]^{3+}$ cation, three BF_4^- counteranions, one of which was disordered, and a H_2O of crystallization in the asymmetric unit. As with the previous complexes, the ligand had a stretched out shape with a Zn(II) ion bound to each

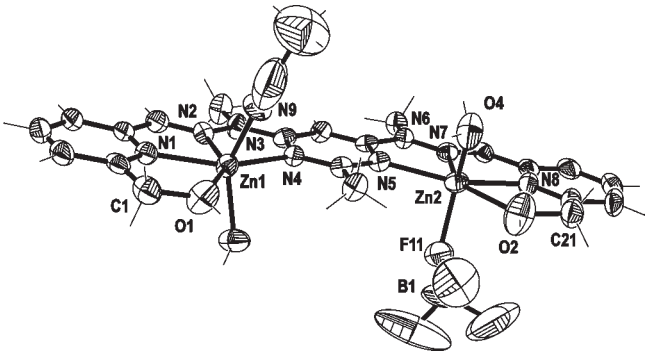

Figure 14. View of $[Zn_2\mathbf{1}(BF_4)(CH_3CN)(H_2O)_2]^{3+}$ cation of complex **8** showing the major component of the disordered hydroxymethyl arm C21−O2 (crystallographic numbering). Thermal ellipsoids drawn at the 50% probability level.

of the coordination sites of **1**. The distance between the centroids of the pyridine rings was 13.21 Å. Both Zn(II) ions displayed a distorted octahedral geometry and were coordinated to the 3 N donors and hydroxymethyl arm of a pym−hyz−py site. A BF_4^- anion and a H_2O molecule were also coordinated to Zn2, while the coordination sphere of Zn1 was completed by a H_2O molecule and a CH_3CN molecule. The hydroxymethyl arm from C21 to O2 was disordered over two sites: one where it was coordinated to Zn2 (site occupancy 0.63) and the other where it was orientated away from Zn2 (site occupancy 0.37). As a result, the O2−Zn2 bond was weaker and therefore longer than the O1−Zn1 bond, at 2.42(2) Å. The partially bound nature of the O2 donor also resulted in the geometry around the Zn2 ion exhibiting some trigonal bipyramidal character, as indicated by the angle between the axial donors O4−Zn2−F11 of 134.7(3)° (Figure 14).

The stronger binding of Zn1 to O1, as opposed to Zn2 to O2, pulled the N1 pyridine ring down slightly, giving the ligand a very slight bow shape. This resulted in a centroid-to-centroid distance between the pyridine rings of only 10.52(8) Å. There was a H-bond between the H_2O of crystallization and the water coordinated to Zn1, with an O3−H···O5 distance of 2.12(13) Å [corresponding to an O3−O5 distance of 2.697(13) Å]. The disorder of the C21−O2 hydroxymethyl arm and one of the BF_4^- counterions meant that no further H-bonding could be characterized.

Comparison of Metal Complex X-ray Structures. X-ray crystallography showed that the hydroxymethyl arms did not interfere with the conformational change of the pym−hyz linkages of **1** upon metal ion coordination. The 2:1 Pb(II) complexes **2**−**4** all showed both hydroxymethyl arms were bound to Pb(II) ions. These complexes were also the longest of the linear complexes, with an average centroid-to-centroid distance between the terminal pyridine rings of 14.09 Å. The 2:1 $Zn(SO_3CF_3)_2$ complex **7** also had both hydroxymethyl arms bound to Zn(II) ions, but had a shorter length of only 12.87 Å due to its distinctly bowed shape. This shape was caused by the difference in H-bonding between the H_2O molecules bound to opposite sides of the Zn(II) coordination spheres. The other 2:1 Zn(II) complex **8** was distorted such that the binding of the hydroxymethyl arms varied from one bound to both bound. Complex **8** had a linear shape, with a length of 13.21 Å.

Comparing the Pb(II) complexes **2** and **4**, and the Zn(II) complexes **7** and **8**, showed that the choice of counterion had

dx.doi.org/10.1021/ic200670w |*Inorg. Chem.* 2011, 50, 7637–7649

little influence on the outcome of the complexation reactions. Likewise, comparing **2** and **3**, and **5** and **6**, showed that solvent also had little impact on the primary structure of the complexes. The counterions and solvent molecules merely competed with H_2O to complete the coordination sphere of the metal ion bound to **1**. As a result, they did not affect the conformational change of the ligand; however, the coordination of four H_2O molecules to the Zn(II) ions in complex **7** did affect the overall shape of the complex molecule. The counterions mainly affected the stacking arrangement of the complex molecules by providing H-bonding donors and acceptors, which linked the complex molecules together as 1D chains, such as complexes **3** and **4**, or 2D networks, such as complex **7**. The molecules of complex **2** were arranged as a 1D chain through H-bonding and anion$-\pi$ interactions, both involving ClO_4^- anions.

As expected, **5** and **6** showed that it was possible to create a [2 × 2] grid structure despite the coordination of the hydroxymethyl arms, if a large enough metal ion was used. The Pb(II) ions in complexes **5** and **6** were eight coordinate, with bonds to hydroxymethyl arms on both ligands and to a ClO_4^- anion. NMR spectroscopy showed that only the grid structure was present in solution, ruling out formation of an unsymmetrical mono-Pb(II) structure such as those seen when reacting Cu(II) and **1** in a 1:1 ratio.[11] Grid formation was possible with Pb(II) due to its large coordination sphere, which allowed the eight coordinate Pb(II) ions in complexes **5** and **6** to accommodate two molecules of **1** despite coordination of the hydroxymethyl arms to the Pb(II) ions. The coordination of the hydroxymethyl arms did, however, cause a twist in the ligand backbone, which resulted in individual grids of **5** and **6** being heavily distorted. This is unlike the [2 × 2] grids, which have been made with previous pym−hyz strands, and Pb(II) ions, which have had square structures.[2,14,19]

Unfortunately, the solid-state structure of the 1:1 $Pb(SO_3CF_3)_2$ complex could not be ascertained. Single crystals were repetitively grown by slow diffusion of diethyl ether into CH_3CN solutions of the 1:1 $Pb(SO_3CF_3)_2$ and **1** mixture. These crystals appeared to be of good quality and showed extinction under polarized light; however, none were unable to produce an X-ray diffraction pattern. The ^1H NMR of the complex suggested that its structure in solution was similar to that of the 1:1 $Pb(ClO_4)_2$ complex.

Although Zn(II) has been successfully used to form [2 × 2] square grids with other pym−hyz strands,[2,19] no such complexes were produced from ligand **1** and $Zn(SO_3CF_3)_2$ or $Zn(BF_4)_2 \cdot H_2O$. The fact that addition of a one molar equivalence of either of the Zn(II) salts to **1** did form a clear yellow solution suggested that there was some initial interaction between the Zn(II) ions and **1**. However, the NMR results suggested that no complexes were formed in solution, and the ligand precipitated back out of the solution within minutes. The lack of a [2 × 2] grid complex is the result of the hydroxymethyl arms preventing grid formation by saturating the smaller coordination sphere of the Zn(II) ions. It is interesting though that the 1:1 reaction did not produce either a mixture of the 2:1 complex and unreacted **1** or a 1:1 mono-Zn(II) complex similar to those seen with Cu(II) ions.[11]

CONCLUSION

Complexation of **1** with $Pb(ClO_4)_2 \cdot 3H_2O$ on a 1:1 metal/ligand ratio resulted in an unusually distorted [2 × 2] grid structure both in solution and in the crystalline state, despite coordination of the terminal hydroxymethyl arms of **1** to the Pb(II) ion. This validated our hypothesis that grid formation was possible with ligand **1**, even with interference from donors on the terminal pyridine rings of a pym−hyz strand, if a large enough metal ion was used.

$Pb(ClO_4)_2 \cdot 3H_2O$, $Pb(SO_3CF_3)_2 \cdot H_2O$, $Zn(SO_3CF_3)_2$, and $Zn(BF_4)_2$ were all successfully reacted with **1** in a 2:1 metal/ligand ratio in CH_3CN, resulting in linear complexes with both pym−hyz bonds rotated to a cisoid conformation. The choice of counterion or solvent had little influence on the primary structure of the complexes, only affecting the intermolecular interactions by providing H-bonding donors and acceptors and by affecting the packing arrangement of the complexes.

The range of complexes produced thus far shows that **1** is a diverse ligand, which can bind to a wide variety of metal ions to form grid structures as well as linear and mono coordinated bent structures. Special consideration must be given to the size of the metal ion used to generate the supramolecular structural outcome that is desired. The formation of the Pb(II) [2 × 2] grid structures shows that two molecules of **1** can bind to the same ion, even with interference from the hydroxymethyl arms, as long as a large enough metal ion is used. Therefore, the addition of hydroxymethyl arms to the pym−hyz molecular strand has bestowed on ligand **1** the ability to form various self-assembled architectures, which are dependent on the metal ion used. In this way, the addition of functional groups able to coordinate to metal ions allows control of the self-assembly of pym−hyz complexes.

ASSOCIATED CONTENT

Supporting Information. X-ray data in CIF format. Bond length and angle data of complexes **2**−**8**. This material is available free of charge via the Internet at http://pubs.acs.org.

AUTHOR INFORMATION

Corresponding Author

*Phone: (+64) 3-479-7918. Fax: (+64) 3-479-7906. E-mail: lhanton@chemistry.otago.ac.nz.

ACKNOWLEDGMENT

We thank the Department of Chemistry, University of Otago, and the New Economic Research Fund of the Foundation for Research, Science, and Technology (NERF Grant No UOO-X0808) for financial support.

REFERENCES

(1) Lehn, J.-M. *Chem.-Eur. J.* **2006**, *12*, 5910–5915.

(2) Stadler, A.-M.; Kyritsakas, N.; Graff, R.; Lehn, J.-M. *Chem.-Eur. J.* **2006**, *12*, 4503–4522.

(3) (a) Schmitt, J.-L.; Stadler, A.-M.; Kyritsakas, N.; Lehn, J.-M. *Helv. Chim. Acta* **2003**, *86*, 1598–1624. (b) Schmitt, J.-L.; Lehn, J.-M. *Helv. Chim. Acta* **2003**, *86*, 3417–3426. (c) Gardinier, K. M.; Khoury, R. G.; Lehn, J.-M. *Chem.-Eur. J.* **2000**, *6*, 4124–4131.

(4) (a) Stadler, A.-M.; Ramírez, J.; Lehn, J.-M. *Chem.-Eur. J.* **2010**, *16*, 5369–5378. (b) Stadler, A. M.; Puntoriero, F.; Nastasi, F.; Campagna, S.; Lehn, J.-M. *Chem.-Eur. J.* **2010**, *16*, 5645–5660.

(5) Ramírez, J.; Stadler, A.-M.; Brelot, L.; Lehn, J.-M. *Tetrahedron* **2008**, *64*, 8402–8410.

(6) (a) Kay, E. R.; Leigh, D. A.; Zerbetto, F. *Angew. Chem., Int. Ed.* **2007**, *46*, 72–191. (b) Balzani, V.; Credi, A.; Raymo, F. M.; Stoddart, J. F. *Angew. Chem., Int. Ed.* **2000**, *39*, 3348–3391.
(7) Schneider, H.-J.; Strongin, R. M. *Acc. Chem. Res.* **2009**, *42*, 1489–1500.
(8) (a) Ulrich, S.; Petitjean, A.; Lehn, J.-M. *Eur. J. Inorg. Chem.* **2010**, 1913–1928. (b) Petitjean, A.; Khoury, R. G.; Kyritsakas, N.; Lehn, J.-M. *J. Am. Chem. Soc.* **2004**, *126*, 6637–6647.
(9) Chaur, M.; Collado, D.; Lehn, J.-M. *Chem.-Eur. J.* **2011**, *17*, 248–258.
(10) Lao, L. L.; Schmitt, J.-L.; Lehn, J.-M. *Chem.-Eur. J.* **2010**, *16*, 4903–4910.
(11) Hutchinson, D. J.; Hanton, L. R.; Moratti, S. C. *Inorg. Chem.* **2010**, *49*, 5923–5934.
(12) (a) Maeda, S.; Hara, Y.; Nakamaru, S.; Hashimoto, S. *Polymers* **2011**, *3*, 299–313. (b) Huck, W. T. K. *Mater. Today* **2008**, *11*, 24–32.
(13) Cao, X.-Y.; Harrowfield, J.; Nitschke, J.; Ramirez, J.; Stadler, A.-M.; Kyritsakas-Gruber, N.; Madalan, A.; Rissanen, K.; Russo, L.; Vaughan, G.; Lehn, J.-M. *Eur. J. Inorg. Chem.* **2007**, 2944–2965.
(14) Ruben, M.; Breuning, E.; Barboiu, M.; Gisselbrecht, J.-P.; Lehn, J.-M. *Chem.-Eur. J.* **2003**, *9*, 291–299.
(15) Tielmann, P.; Marchal, A.; Lehn, J.-M. *Tetrahedron Lett.* **2005**, *46*, 6349–6353.
(16) Winter, S.; Seichter, W.; Weber, E. *Z. Anorg. Allg. Chem.* **2004**, *630*, 434–442.
(17) Yilmaz, V. T.; Guney, S.; Andac, O.; Harrison, W. T. A. *Polyhedron* **2002**, *21*, 2393–2402.
(18) Ramirez, J.; Stadler, A.-M.; Harrowfield, J. M.; Brelot, L.; Huuskonen, J.; Rissanen, K.; Allouche, L.; Lehn, J.-M. *Z. Anorg. Allg. Chem.* **2007**, *633*, 2435–2444.
(19) (a) Barboiu, M.; Ruben, M.; Blasen, G.; Kyritsakas, N.; Chacko, E.; Dutta, M.; Radekovich, O.; Lenton, K.; Brook, D. J. R.; Lehn, J.-M. *Eur. J. Inorg. Chem.* **2006**, 784–792. (b) Giuseppone, N.; Schmitt, J.-L.; Lehn, J.-M. *J. Am. Chem. Soc.* **2006**, *128*, 16748–16763. (c) Ruben, M.; Lehn, J.-M.; Vaughan, G. *Chem. Commun.* **2003**, 1338–1339.
(20) Harrowfield, J. *Helv. Chim. Acta* **2005**, *88*, 2430–2432.
(21) (a) Otwinowski, Z.; Minor, W. Processing of X-Ray Diffraction Data Collected in Oscillation Mode. In *Methods in Enzymology*; Carter, C. W., Jr., Sweet, R. M., Eds.; Academic Press: New York, 1997; Vol. 276, pp 307−326. (b) *SAINT V4, Area Detector Control and Integration Software*; Siemens Analytical X-Ray Systems Inc.: Madison, WI, 1996.
(22) Sheldrick, G. M. *SADABS, Program for Absorption Correction*; University of Göttingen: Göttingen, Germany, 1996.
(23) Sheldrick, G. M. *Acta Crystallogr., Sect. A* **1990**, *46*, 467–473.
(24) Altomare, A.; Burla, M. C.; Camalli, M.; Cascarano, G. L.; Giacovazzo, C.; Guagliardi, A.; Moliterni, A. G. G.; Polidori, G.; Spagna, R. *J. Appl. Crystallogr.* **1999**, *32*, 115–119.
(25) Sheldrick, G. M. *SHELXL-97, Program for the Solution of Crystal Structures*; University of Göttingen: Göttingen, Germany, 1997.
(26) Farrugia, L. J. *J. Appl. Crystallogr.* **1999**, *32*, 837–838.
(27) Spek, A. L. *Acta Crystallogr., Sect. A* **1990**, *46*, C34.
(28) (a) Macrae, C. F.; Edgington, P. R.; McCabe, P.; Pidcock, E.; Shields, G. P.; Taylor, R.; Towler, M.; van de Streek, J. *J. Appl. Crystallogr.* **2006**, *39*, 453–457. (b) Bruno, I. J.; Cole, J. C.; Edgington, P. R.; Kessler, M. K.; Macrae, C. F.; McCabe, P.; Pearson, J.; Taylor, R. *Acta Crystallogr., Sect. B* **2002**, *58*, 389–397.
(29) Allen, F. H.; Davies, J. E.; Galloy, J. J.; Johnson, O.; Kennard, O.; Macrae, C. F.; Mitchell, E. M.; Mitchell, G. F.; Smith, J. M.; Watson, D. G. *J. Chem. Inf. Comput. Sci.* **1991**, *31*, 187–204.